Automated High-Resolution Satellite Image Registration Using Supraglacial Rivers on the Greenland Ice Sheet

Article *in* IEEE Journal of Selected Topics in Applied Earth Observations and Remote Sensing · November 2016

DOI: 10.1109/JSTARS.2016.2617822

4 authors:

Kang Yang
University of California, Los Angeles
27 PUBLICATIONS **99** CITATIONS
SEE PROFILE

Leif Karlstrom
University of Oregon
46 PUBLICATIONS **224** CITATIONS
SEE PROFILE

Laurence C. Smith
University of California, Los Angeles
147 PUBLICATIONS **5,345** CITATIONS
SEE PROFILE

Manchun Li
Nanjing University
146 PUBLICATIONS **439** CITATIONS
SEE PROFILE

Automated High-Resolution Satellite Image Registration Using Supraglacial Rivers on the Greenland Ice Sheet

Kang Yang, Leif Karlstrom, Laurence C. Smith, and Manchun Li

***Abstract*—High-resolution satellite imagery raises new prospects for detailed study of the Greenland ice sheet (GrIS) surface processes and ice discharge. However, dramatic spatiotemporal variability of ice surface reflectance and features poses significant challenges for registration of satellite imagery. This study proposes a new feature-based registration method to register high-resolution panchromatic images of the ice sheet ablation zone. Its idea is to use relatively stable supraglacial rivers as tie points for automated image registration. A first demonstration is made using WorldView-1/2/3 panchromatic images (spatial resolution 0.5 m) as follows: first, supraglacial rivers are delineated using spectral analysis, nonlocal means denoising, Gabor filtering, and path opening. Next, buffer and overlay tools are combined to generate an area of interest and eliminate tie point outliers, yielding subset of high-confidence tie points for registration. Finally, a coherent point drift algorithm is applied to match these tie points and implement registration. Results show that the proposed method demonstrates good performance, despite a heterogeneous ice surface background that complicates river delineation. Accuracy of image registration negatively correlates with seasonal spatiotemporal variability of supraglacial river patterns, suggesting that for the best results, repeat images and time-adaptive techniques should be used. For time-stable meltwater channels, however, the method offers a novel, automated way to register high-resolution satellite imagery of the GrIS ablation zone. Well-registered ice surface high-resolution images that reveal short-term (1–2 week) variations in surface melting rate affect channel morphology (drainage densities and channel widths) significantly, whereas a signal from background advection by flowing ice is not apparent.**

***Index Terms*—Greenland ice sheet, image registration, river delineation, supraglacial river, WorldView.**

Manuscript received April 15, 2016; revised July 15, 2016, September 13, 2016, and September 20, 2016; accepted October 3, 2016. This work was supported in part by the NASA Cryosphere Program under Grant NNX14AH93G managed by Dr. Thomas Wagner, and in part by the National Natural Science Foundation of China under Grant 41501452. WorldView imagery and geospatial support for this work was provided by the Polar Geospatial Center, University of Minnesota, under National Science Foundation Division of Polar Programs Awards 1043681 and 1559691.

K. Yang is with the Department of Geography, University of California, Los Angeles, Los Angeles, CA 90095 USA, and also with the Department of Geographic Information Science, Nanjing University, Nanjing 210023, China (e-mail: yangkangnju@gmail.com).

L. Karlstrom is with the Department of Earth Sciences, University of Oregon, Eugene, OR 97403 USA (e-mail: leif@uoregon.edu).

L. C. Smith is with the Department of Geography, University of California, Los Angeles, Los Angeles, CA 90095 USA (e-mail: lsmith@geog.ucla.edu).

M. Li is with the Department of Geographic Information Science, Nanjing University, Nanjing 210023, China (e-mail: manchunli_geo@126.com).

Color versions of one or more of the figures in this paper are available online at http://ieeexplore.ieee.org.

Digital Object Identifier 10.1109/JSTARS.2016.2617822

I. Introduction

THE Greenland ice sheet (GrIS) has experienced extensive mass loss in recent decades, thus becoming an important contributor to global sea level rise [1]. Ice sheet models (i.e., surface mass balance and ice discharge models) and satellite observations are two primary approaches used to analyze the GrIS mass balance [2]. The latter can provide direct investigations of hydrological/glaciological processes on the ice surface and has received growing attentions in recent years [3]–[5].

Multiresolution (0.5 m–1 km), multisensor (e.g., optical, synthetic aperture radar (SAR), and LiDAR sensors), and multitemporal satellite images have been widely used in GrIS studies [5]. A growing availability of high-resolution optical imagery, such as IKONOS, GeoEye-1, QuickBird, SPOT-5/6, WorldView-1/2/3, and unmanned aerial vehicle (UAV) imagery, has raised the prospects of studying GrIS hydrology in great detail [6]. However, the GrIS surface is a highly dynamic hydrological/glaciological environment, characterized by different surfaces (e.g., meltwater, ice, firn, slush, and wet/dry snow) [7], supraglacial lake formation/drainage [8], supraglacial river incision [9], moulin formation/closure [10], uneven eolian dust distribution [11], different melt intensities [12], and variable ice flow velocities [13]. These complex conditions pose significant challenges for analyzing high-resolution images of the ice surface and consequently impede improved understanding of the GrIS response to climate change.

Image registration is an initial but crucial step in analyzing high-resolution satellite imagery, which aims to spatially align images taken at different times, from different viewpoints, and/or by different sensors [14]. In particular, registering high-resolution ice surface imagery is important for revealing key physical processes occurring on the ice surface during melt seasons. For example, well-registered images can be used to study supraglacial river network evolution, supraglacial lake filling/drainage, ice flow velocity, fluvial erosion on the ice surface, and moulin formation, consequently revealing the response of GrIS to climate change. In the registration process, one image (i.e., the master image) is used as the reference for all other images (i.e., slave images). Conjugated feature points that are visible on both the master and slave images are used as tie points (TPs) and, subsequently, an optimal registration model is developed based on these TPs [15]. After registration, multitemporal images are spatially aligned and thus change delineation and other analyses can then be conducted, finally revealing important patterns or ongoing processes from satellite observations.

There are two approaches for obtaining conjugated feature points, i.e., intensity-based and feature-based methods [14]. Intensity-based methods aim to align whole images (or subimages) by computing similarity measures (e.g., cross correlation and mutual information) among pixels and then optimize these measures for different image transformations [14]. Most of the intensity-based methods are impractical or require substantial updates when applied to register complicated satellite imagery because they are sensitive to image intensity and gradient changes [14], [16]. Feature-based methods, in contrast, perform better to registration of multitemporal, multisensor satellite images. In general, abundant features (e.g., buildings, road networks, shorelines, and lakes) are found in terrestrial satellite images, which can be delineated and used as target features to generate TPs. However, target features in satellite images are difficult to extract and match. To address this problem, much effort has focused on delineating and employing different types of features (points, lines, and regions) to register satellite images [14]. For example, region corners [17], line intersections [18], [19], and region centroids [15] are all representative point features that can be extracted from images and used to create high confident TPs for image registration [14]. An improved scale invariant feature transform was first used to obtain initial point matching features; then, the initial matching features were refined by exploring their spatial relationships, yielding high confident TPs for image registration [20]. Linear road segments were separately detected from optical and SAR images using linear segment detector and Hough transform, and then an iterative and coarse-to-fine approach was applied to successfully register SAR images with optical images [19]. A classic region-based approach combined an invariant moment shape descriptor with improved chain-code matching to establish correspondences between potentially matched regions detected from two images [21]. Notably, most of the feature-based image registration methods consider targets features are stable over time. However, substantial changes can be observed in variable landscapes. It is more challenging to register multitemporal images due to variability of features captured by imagery. As an example, vector road dataset was used to generate ground control points, which were then used to register satellite images via a road geometric modeling approach [22]. In the dynamic Arctic, centers of lakes are considered stable even if their shorelines are not; thus, those center points are used as TPs to register Arctic satellite images [15]. However, critical problems still remain, particularly when knowledge about target features is poor and/or dramatic changes occur among multitemporal images.

The complex and highly dynamic ice surface gives rise to even more challenging problems. First, variable ice surface topography poses a considerable challenge to effective feature detection. Second, the ice surface changes dramatically (during the melt season) [3], [5] and thus lacks stable features to be used as TPs. As an example, Fig. 1 shows two WorldView (WV) panchromatic images of a small area located in the southwest of the GrIS (elevation is ∼1200 m), acquired in July 2015. There is an average ∼19 pixel (i.e., 9.5 m) offset between these two images. Although these two images were acquired only 13 days apart, drastic appearance changes are observed owing to variations in melt status and surface cover (e.g., snow, eolian dust, and meltwater). These significant variations render the use of intensity-based image registration methods impractical because similarity measures are sensitive to intensity variations [14], [16].

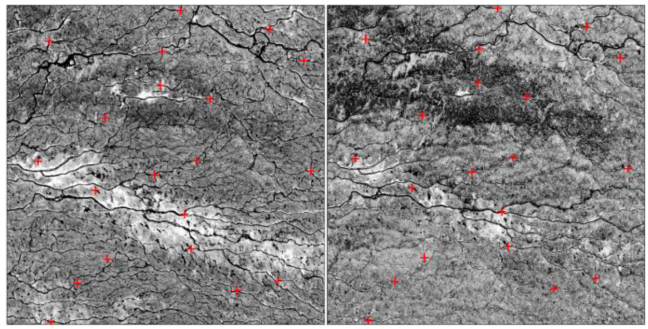

(a) (b)

Fig. 1. Sample WorldView-1 (WV1) and WorldView-3 (WV3) panchromatic images (both with spatial resolution 0.5 m), covering an area of 0.56 km^2 of the southwest of the GrIS where supraglacial rivers are prevalent: (a) WV1 image acquired on 18 July 2015, and (b) WV3 image acquired on 31 July 2015. A total of 20 pairs of manually identified TPs (red crosses) have an average offset of ∼19.0 ± 1.8 pixels (9.5 ± 0.9 m).

As such, we advocate that supraglacial rivers, the only visible surface features in the two WV images (see Fig. 1) and the most notable and pervasive features in the GrIS high-resolution images during melt seasons [23], [24], can be used to register ice surface images. It should be noted that crevasses are widely distributed below 1100 m in the southwest of the GrIS and have important impacts on the ice surface [25]. However, the focus of this study is rivers and study sites above 1200 m, where very few crevasses are distributed. Fig. 1 shows that the overall pattern of supraglacial rivers is relatively stable, even though the ice surface changes substantially. This stability is due to a combination of relatively slow underlying ice flow and bedrock topography expressed on the surface of the ice sheet, which controls supraglacial drainage basin locations [9]. As such, it is possible to delineate and employ these rivers as conjugated features, in order to subsequently register ice surface images.

This paper proposes an automated method to register high-resolution ice surface images using supraglacial rivers. It is a feature-based registration method, consisting of two main steps: 1) delineation of supraglacial rivers from high-resolution images using spectral analysis, nonlocal means denoising, Gabor filtering, and path opening processes; and 2) generation of high-confidence TPs from these supraglacial rivers using a buffer-and-overlay approach and a robust point pattern registration algorithm.

II. Methods

Two key problems need to be addressed to develop a river-based image registration method. First, it is very challenging to delineate supraglacial river networks from high-resolution satellite images because of the aforementioned complex ice surface characteristics. Second, although main-stems are stable, details of supraglacial river networks obtained from different dates still differ considerably (see Fig. 1), which can cause a number of

erroneous TPs and consequently reduce the final registration performance. In this study, we addressed the first problem using two-step preprocessing, and solved the second problem using two conventional geographic information system (GIS) tools and a robust point pattern matching algorithm.

Spatial offsets among ice surface images are primarily caused by two effects. The first is a "raw" offset due to image acquisition conditions. This offset is similar to that reported in regular terrestrial image registration studies [15]. The second offset is caused by advection of rivers by underlying ice flow. Although lateral offset of terrestrial topographic features does occur (for example, by strike-slip faults [26]), it is generally negligible for terrestrial images. GrIS surface flow is driven by variations in the local driving stress, which on large scales are set by surface slope variations toward the ice margin [13], [27]. Thus, there will be offsets among the ice surface images acquired from different dates even if the raw offsets do not exist. Most of the GrIS ice flow studies focus on long-term (e.g., annual or interseasonal) velocity variations over large areas using moderate-resolution SAR or optical satellite images [13]. In contrast, high-resolution imagery is more appropriate for revealing short-term (e.g., 1–30 days) local ice surface variations. We have found that it is difficult to distinguish the ice-flow-induced offsets from the raw offsets in high-resolution images. Therefore, we focus here on eliminating the overall offsets among high-resolution images and only briefly illustrate the potential impacts of ice flow on high-resolution image registration.

WV panchromatic images (spatial resolution 0.5 m) were used as experimental data. These images were orthorectified based on the satellite positioning model (also known as the rational function model) and projected into a polar stereographic coordinate system using the code developed by the Polar Geospatial Center [9]. These orthorectified images were roughly registered (offset is 19.0 $\pm$ 1.8 pixels, or 9.5 $\pm$ 0.9 m, see Fig. 1), which suggests sufficient geolocation accuracy of WV images as no ground control points can be applied. However, supraglacial meltwater channels are very narrow ($\sim$1–30 m or less) [6], [23], [28], [29]. The rough geolocation accuracy ($\sim$10 m offset) hinders ice surface change detection and thus further accurate registration is required.

A. Preprocessing

1) Eliminating Image Background Using High-Pass Discrete Fourier Transform (DFT): Active supraglacial rivers manifest as narrow, dark, linear features with abrupt bright channel banks, which can be considered as high-frequency information in high-resolution images, while locally different ice surfaces (e.g., bright snow and eolian dust patches/zones, see Fig. 1) belong to low-frequency information in the image. This local image background can induce noise and thus reduces supraglacial river delineation accuracy [6].

To address this problem, we used DFT to construct a spectral filter to remove the low-frequency image background [30]. DFT spectral power density is visualized using radial frequencies to construct a 1-D spectrum (see Fig. 2). We found that a high-pass filter that ramped up between $1/200$ and $1/10$ m^{-1} (the frequency band in which supraglacial rivers are

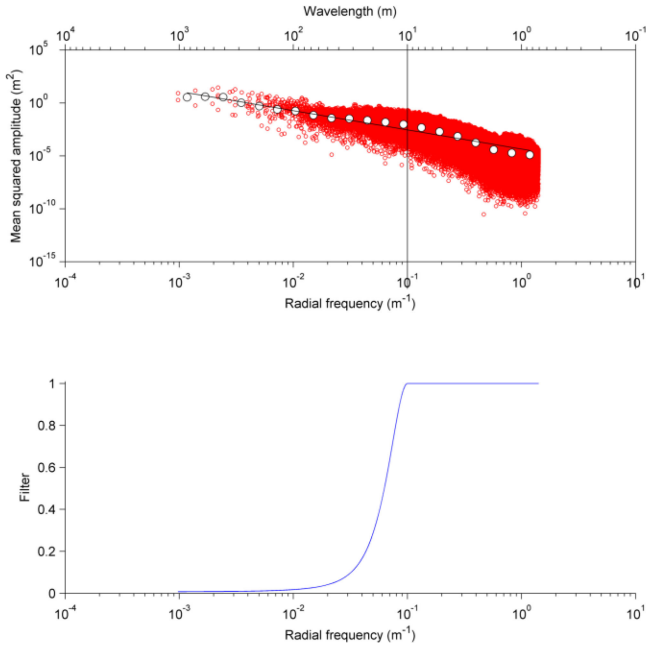

Fig. 2. One-dimensional DFT power spectra for the panchromatic image of Fig. 1(a). Red circles indicate the spectral amplitude range of the input image and black circles indicate the corresponding binned averages. A high-pass spectral filtering is designed to filter out the low-frequency ice surface background, with filter range (ramp between $1/200 - 1/10$ m^{-1}) shown in the below panel.

dominant topographic features on the ice sheet surface [9]) performs well to remove image background and simultaneously to enhance river features. The original WV image and the high-pass filtered result are shown in Fig. 3. Rivers are significantly enhanced from the image background after high-pass DFT filtering (see Fig. 3(a) and (b)). Fig. 3(c) shows the remaining low-frequency image background that has been successfully eliminated. However, abundant high-frequency noise remained in the high-pass filtered image (see the zoomed image in Fig. 3(b)). Using a band-pass DFT filter would eliminate this high-frequency noise as well as the low-frequency image background [9] but would simultaneously eliminate considerable parts of the high-frequency river information. Therefore, the high-pass filter was applied here instead of the band-pass filter, and a denoising algorithm was subsequently applied to eliminate high-frequency noise without losing useful river information.

2) Denoising Image Using Optimized Block-Wise Nonlocal Means (OBNLM) Filter: OBNLM was originally developed for high-resolution ultrasound images, using a Bayesian framework to derive a nonlocal-means filter adapted to a relevant ultrasound noise model [31]. A comprehensive comparison of six denoise filters showed that the OBNLM filter performed the best at reducing noise and smoothing high-resolution ultrasound images [32]. Although panchromatic satellite sensors are different from ultrasound sensors and the OBNLM filter was originally designed to eliminate speckle noise (which is not present in panchromatic optical images), we show that the OBNLM filter is useful for processing a rough ice surface. Specifically, the Greenland ice surface is locally variable due to different melt intensities, leading to significant roughness of the image

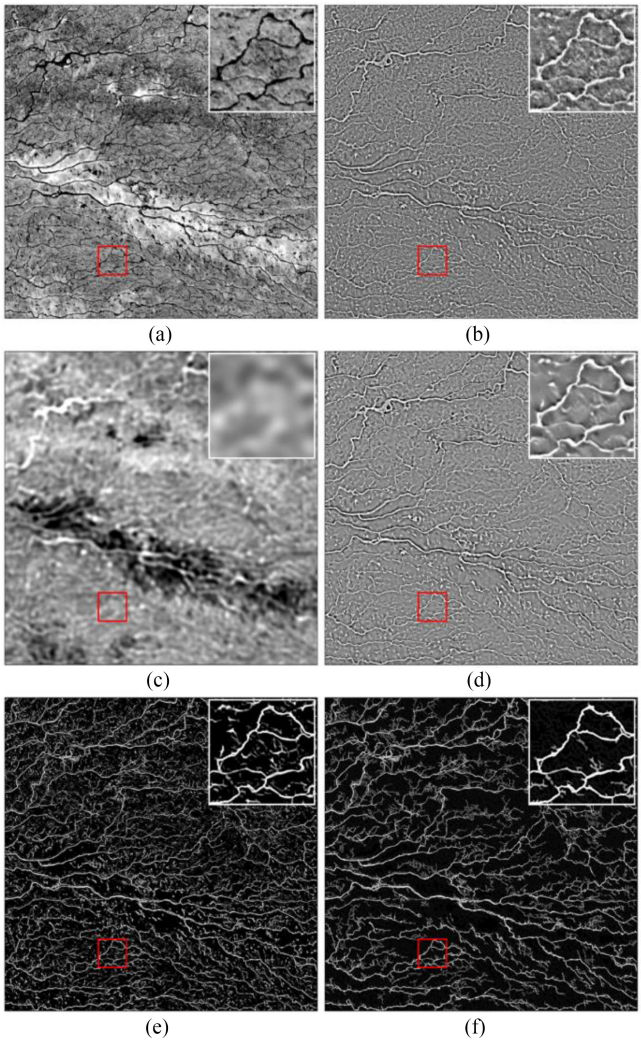

Fig. 3. Supraglacial river enhancement in WV1 high-resolution panchromatic image acquired 18 July 2015. (a) Raw panchromatic image, (b) image after high-pass DFT filtering, (c) subtraction of (b) from (a) confirming removal of local heterogeneities from (a), (d) denoised image after nonlocal means filtering of (b), (e) Gabor filtering of (d), and (f) river enhancement result after application of a path opening algorithm to (e). A close-up of the red box area is shown in each upper right corner.

surface (see Fig. 3(b)). The OBNLM filter can eliminate noise and smooth the high-pass filtered satellite image (see Fig. 3(d)). Furthermore, OBNLM can accurately preserve edges and structural details of the image and thus is very useful for eliminating noise and preserving rivers [32]. Three parameters were required to conduct OBNLM filtering: search area size $(2M_1 + 1)^2$; patch size $(2M_2 + 1)^2$; and smooth parameter h. M_1 determines the spatial extent in which to search for potentially similar image patches, which was set to 7 in this study. M_2 determines the patch size for conducting similarity calculations, which was set to 3. h is a key parameter for determining the smooth intensity. If h is set too high, the useful structure (i.e., rivers) will be eliminated and shown in the residual image; if h is set too low, noise will remain in the denoised image. In this study, h was set to 0.7. Another example is presented in Fig. 4, which shows that

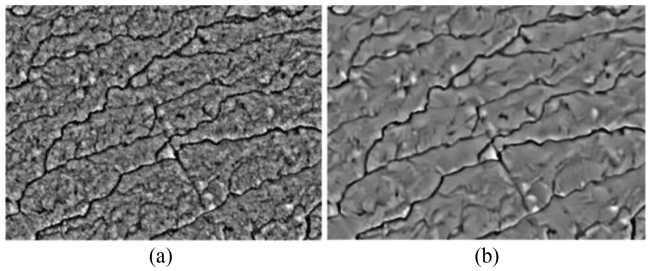

Fig. 4. (a) WV1 high-resolution panchromatic image after high-pass DFT filtering, and (b) denoised image after nonlocal means filtering of (a).

the OBNLM filter effectively eliminates background noise and enhances river characteristics from local ice surface background.

B. Supraglacial River Delineation

Supraglacial rivers were efficiently enhanced and showed significant differences from the image background after preprocessing. Subsequently, complete river networks could be delineated using the method proposed in [33]. This method employed Gabor filtering to enhance river cross sections and path opening to lengthen the river channel continuity. The thickness of the Gabor filter, w, was set to 2 to enhance all the narrow rivers. Rivers were more effectively discerned from the image background after Gabor filtering but they could be easily corrupted owing to significant gray value variation along river courses (see Fig. 3(e)). Path opening, a flexible morphological operator, was then used to lengthen the longitudinal channel continuity. A key parameter in path opening was $L_{\min}$, which determined the minimum path to be enhanced. In this study, $L_{\min}$ was set to 20 m (i.e., 40 WV panchromatic pixels) and consequently all rivers longer than this length were consistently enhanced and discerned from the image background (see Fig. 3(f)). The output image after path opening was a normalized image, yielding a gray value range of [0, 255]. Finally, a global threshold (t) was applied to create binary river masks from this river enhanced image.

Numerous rivers are detected from high-resolution WV images and thus an efficient vectorization method is required to produce vector river products from these river masks. The ArcScan vectorization function in the ArcGIS software was used for this purpose, with no extra manual modifications or clean-ups applied. Default vectorization settings were used and "Generate Features" tool was applied to convert river pixels into vectorized river polylines. The river delineation results for the two images in Fig. 1 are shown in Fig. 5(a) and (b).

C. Image Registration Based on Supraglacial River Points

1) Selecting TPs Using Buffer and Overlay Operations: The ice surface undergoes significant changes during melt seasons [6]. Although supraglacial rivers are relatively stable, some drainage pattern changes are still observed. As an example, Fig. 5(c) overlays supraglacial rivers delineated from Fig. 1(a) and (b), suggesting that a large portion of river networks is basically stable over a period of 13 days (July 18–31). However,

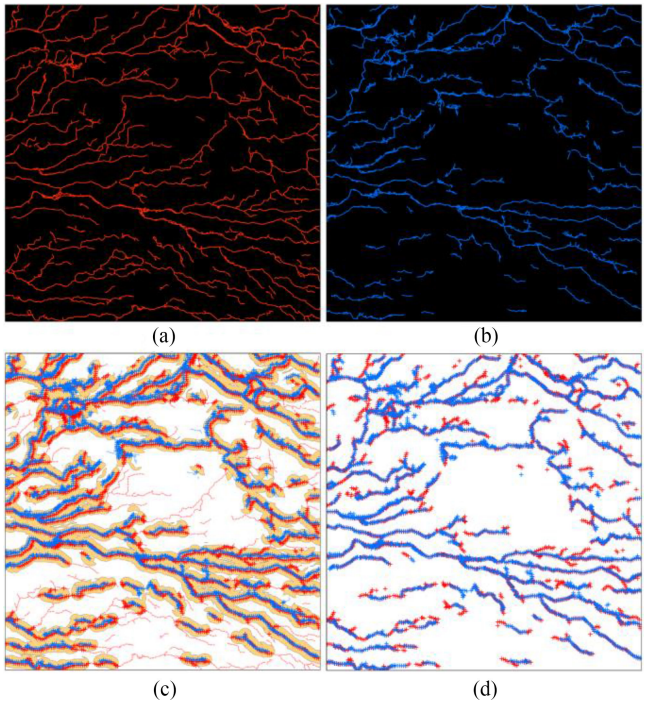

Fig. 5. Final supraglacial river delineation results for (a) 18 July 2015, WV1 and (b) 31 July 2015, WV3. A simple threshold of 35 is applied to classify the normalized river enhancement images (pixel values range from 0 to 255) (c) AOI (yellow) and potential TPs (red and blue crosses) derived from a 15 m buffer applied to (a) and (b), with rivers outside AOI eliminated (dash red and blue lines). A CPD algorithm is applied to register the two point sets in (c), and (d) final registration result.

considerable portions of the river network were different, which can be attributed to variations in melt status, surface cover, and ice flow. This could lead to false matches due to outliers and missing points and also increase computational costs during the subsequent registration process.

To mitigate this temporal change problem, a combination of two simple GIS tools, buffer and overlay, was proposed to eliminate rivers and to generate an area of interest (AOI) [34]. First, a user-specified parameter, buffer distance, was applied to both master and slave images and two buffered areas were obtained. Second, an overlay operation was applied to the two buffered areas and their intersection area was obtained and used as an AOI. Third, this AOI was considered as the potential area that provided correct TPs, and thus only the rivers located in the AOI were kept. Fourth, points were created along the resultant AOI river courses at equal intervals, which were used as potential TPs. This AOI (i.e., buffer and overlay) approach successfully constrained TP selection and reduced potential mismatches (see Fig. 5(c)).

Finally, another user-specified parameter, TP ratio (R_{tp}), was proposed to evaluate the match between the number of TPs obtained from master and slave images. R_{tp} is defined as N_1/N_2, where N_1 (N_2) is the number of TPs obtained from the slave (master) image. If river networks are the same in the master and slave images, $R_{\mathrm{tp}} = 1$; otherwise, some interference points will be included in the AOI and will act as outliers, causing R_{tp} to deviate from 1. Notably, some other factors (e.g., sun inclination, camera angle, and sensor type) can also lead to different river representations in satellite images and thus contribute to R_{tp} variations. The possible effect of these factors has not been explored, but we suspect that their impacts are slight compared to those of actual spatiotemporal river changes and thus neglect them here.

2) Registration of River Point Sets Using Coherent Point Drift (CPD): Two point sets were obtained after the AOI processing (see Fig. 5(c)). These two point sets can be used as inputs for a point set registration algorithm to recover the transformation that maps one point set to the other. Although the AOI constrains the two point sets very well and significantly decreases mismatches [34], a noticeable amount of noise, outliers, and missing points still exist. Therefore, an effective point set registration algorithm should be applied, which is robust to degradations that occur due to imperfect image acquisition and feature extraction. To this end, CPD, a state-of-the-art point set registration algorithm, was employed in this study [35]. CPD considers the alignment of two point sets as a probability density estimation problem. It fits the Gaussian mixture model centroids (representing the first point set) to the data (the second point set) by maximizing the likelihood. The CPD program provides rigid, affine, and nonrigid generalized radial basis function (GRBF) transformation. We used the GRBF transformation since ice flow velocity varies over space and may induce variable offsets. The pairs of points before and after registration were used as TPs for conducting image registration. Fig. 5(d) shows that two supraglacial river patterns were successfully registered using the CPD algorithm.

III. Experimental Results

A. Experimental Settings

WorldView-1/2/3 panchromatic images (provided by DigitalGlobe, Inc., through the Polar Geospatial Center, University of Minnesota, www.pgc.umn.edu), acquired on July 18, 24, and 31, 2015, were used as experimental datasets. The frequency of the high-pass filter ramped up between 1/200 to $1/10\ \mathrm{m}^{-1}$. The three parameters for the OBNLM denoise algorithm were set as $M_1 = 7$, $M_2 = 3$, and $h = 0.7$, respectively. Thickness of the Gabor filter, w, was set to 2. The length parameter of path opening, L_{min}, was set to 20 m (i.e., 40 panchromatic pixels). The global threshold used to classify the normalized river enhancement image (gray value range was [0, 255]) was set to $t = 35$. Buffer distance was set to 15 m to create AOIs and TPs were then created along river courses at 5 m intervals. Nonrigid transformation was selected to conduct the CPD registration.

The Modèle Atmosphérique Régional (MAR) regional climate model [36] was employed to estimate surface melt of the GrIS. MAR is a coupled atmosphere-snow regional climate model with a horizontal resolution of 25 km [37] and available for download from the MAR Greenland Explorer (http://www.cryocity.org/ mar-explorer.html). We used MAR v 3.6 dataset to estimate surface melt for the three WV image acquisition dates.

The Sentinel-1 Greenland product was employed to provide the 2015 annual ice flow velocity [38]. This product is long-term

average velocity (spatial resolution 250 m) and is not concurrent with our study period (July 18–31, 2015). However, at present, long-term velocities are the only available ice flow products for the wide ablation zone of the GrIS [13].

Three comparison methods were used to validate the performance of the described river detection method: a multiscale singularity method [39], a Frangi filter [40], and a multidirectional matched filter [41]. The multiscale singularity method was proposed in [39] to extract river networks from satellite images. This method builds a singularity index that strongly responds to linear structures (e.g., rivers) but weakly responds to image edges. The scale parameter (σ) in this method was set to 3 to capture narrow supraglacial rivers. The Frangi filter is a classic method to detect retinal blood vessels [40]. This method uses the eigenvectors of the Hessian matrix to compute the similarity of one structure to an ideal vessel tube (or river channel). The scale parameter to determine Gaussian derivatives in the Frangi filter was also set to 3. The multidirectional matched filter was first proposed for detecting retinal blood vessels as well [41]. This method is effective for enhancing blood vessels by exploiting the fact that the cross sections of retinal vessels are Gaussian shaped. This idea was adopted in [42] to detect rivers from satellite images. In this study, the scale parameter of the matched filter was set to 2 to effectively enhance narrow supraglacial rivers (<5 pixels).

Four feature-based image registration methods, including speeded-up robust features (SURF) [43], Harris [44], features from accelerated segment test (FAST) [45], and minimum eigenvalue (MinEigen) [46], were used as comparison groups to estimate the performance of the described registration method. The four comparison methods are all state-of-the-art image registration techniques and have been widely used. It is interesting to investigate if those methods can be successfully applied to dynamic ice surface. The four methods are all provided by MATLAB software and we used corresponding MATLAB functions to conduct matching experiments.

B. Test Sites

Four sites were selected as test sites (see Fig. 6 and Table I). The area of each test site was 1500 × 1500 pixels (i.e., 0.56 km^2). In the July 18 image, supraglacial channels drain into a main-stem from the northeast and southwest at Site 1. At the top-right of the image, well-defined rivers develop quickly, whereas in the bottom-left of the image, bright snow patches exist and thus some sparse, discontinuous channels form and flow through the snow patches. At Site 2, rivers flow to the northwest, and eolian dust zones are distributed throughout the middle of the site. Site 3 represents an area where small supraglacial rivers develop particularly well with very little interference. Site 4 shows a watershed divide where headwater channels flow separately to the northwest and southeast, and a very dark eolian dust zone forms at the bottom-right of this site.

July 18 and 24 WV images for Site 1 were used to assess the performance of the proposed method at times when the ice surface was stable (see Fig. 6(a)), while July 18 and 31 images for Site 2–4 were used to assess the performance of the proposed method during periods when considerable changes occurred on the ice surface (see Fig. 6(b)–(d)). In particular, Sites 3 and 4 demonstrate two challenging examples, where dramatic ice surface changes can be observed (e.g., eolian dust zones expand substantially and numerous rivers run dry). In summary, the four sites represent different supraglacial drainage patterns on the ice surface, and demonstrate significant ice surface changes, and can therefore be used to comprehensively assess the performance of the proposed method.

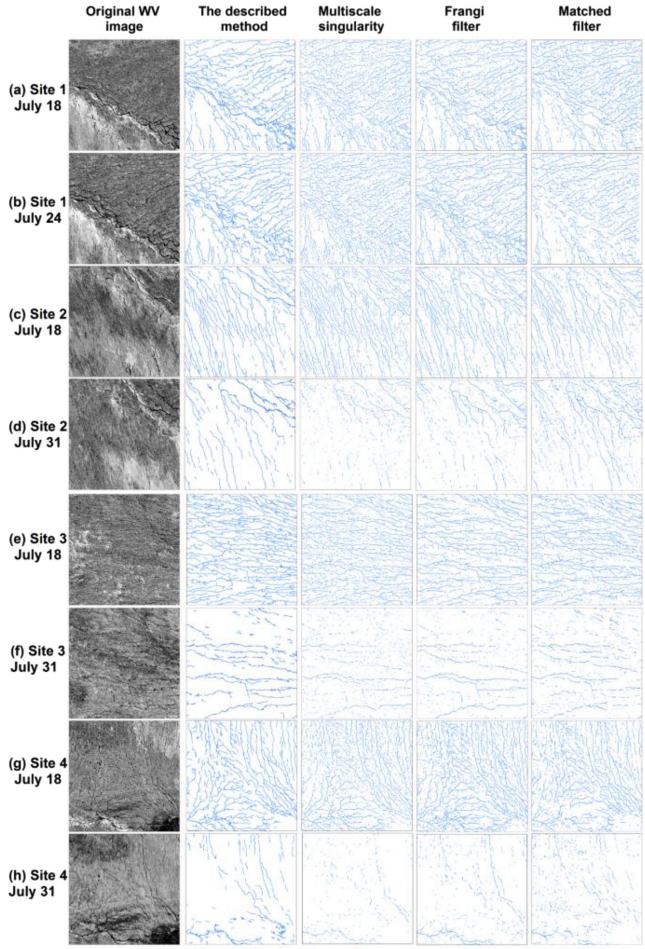

Fig. 6. Original WorldView-1/2/3 (spatial resolution 0.5 m) data (column 1) and corresponding river delineation results for Sites 1–4 (column 2–5) using the described method and three comparison methods.

C. Validation Method

For each test site, a total of 30 TPs were manually identified to evaluate the performance of the proposed method. These TPs were randomly selected at river intersections or inflections covering the images with as even a distribution as possible. The resultant manual TPs were divided into two groups, with each group including 15 TPs. The first group (comparison group) was used to conduct a manual registration and compare with the proposed method, while the second group (validation group) was used to compute the RMSE of registrations and to quantitatively validate the performance of different image registration

TABLE I
SUMMARY STATISTICS OF IMAGE REGISTRATION RESULTS FOR SITES 1–4

Site	Master Image				Slave Image						Ice flow velocity		RMSE (in m)	
	Acquisition date, type	D_d (km/km^2)	Mean river width (m)	TP number	Acquisition date, type	D_d (km/km^2)	Mean river width (m)	TP number	D_d ratio	R_{tp}	Mean (m/a)	Std (m/a)	The proposed method	Manual registration
1	July 18, WV1	52.1	2.9 ± 1.8	6319	July 24, WV3	51.4	2.8 ± 1.6	6630	0.99	1.05	107.6	1.9	1.18	1.36
2		38.5	2.2 ± 0.7	3214		22.2	1.9 ± 0.7	2913	0.58	0.91	107.5	1.4	1.69	1.32
3		58.1	2.1 ± 0.6	3776	July 31, WV2	21.8	1.7 ± 0.5	2990	0.38	0.79	105.5	1.1	2.42	1.86
4		47.0	2.1 ± 0.6	2814		15.8	1.7 ± 0.5	1915	0.34	0.68	105.9	0.8	2.80	2.03

Drainage density D_d, TP number, TP ratio R_{tp}, and RMSE are calculated for evaluation. Manual registration is employed as a comparison method to quantitatively evaluate the performance of the proposed method.

methods. The RMSE is defined as follows:

$$\mathrm{RMSE} = \sqrt{\frac{\sum_{i=1}^{N}\left[(X_i - X_i')^2 + (Y_i - Y_i')^2\right]}{N}} \quad (1)$$

where (X_i, Y_i) and (X_i', Y_i') are two corresponding manual TPs in the registered slave image and the master image, respectively, and N is the number of manual TPs [21].

D. Supraglacial River Delineation Results

The proposed method effectively delineates supraglacial rivers from 0.5 m spatial resolution WV panchromatic images (see Fig. 6). Numerous narrow rivers are successfully delineated from variable image backgrounds. It should be noted that supraglacial river networks are scale-dependent and narrower supraglacial channels (down to 1–2 cm wide) have been observed in the field [29]. These rivers cannot be delineated by 0.5 m WV panchromatic imagery. However, Fig. 6 shows that the WV supraglacial river networks are densely distributed among the ice surface and thus can provide sufficient target features for registration.

All three comparison methods perform well to capture the overall supraglacial river pattern (see Fig. 6). However, supraglacial rivers are discontinuously delineated, with numerous gaps along river courses. In addition, numerous small noisy features are extracted as well. Using a size threshold will eliminate lots of those small features but it will further fragment actual river channels [33]. Among the three comparison methods, the multiscale singularity method mostly fragments river channels and yields abundant noise; the Frangi filter and the matched filter perform better than the multiscale singularity method, offering more continuous channels (particularly for the relatively wide trunks, see Fig. 6(d), (f), and (h)). However, gaps along river courses are still observed, and some narrow headwater channels are not delineated. The described method, however, successfully delineates continuous supraglacial rivers and eliminates most of the small noisy features. Good performance derives from the fact that variable ice surface background is eliminated and small interferences are denoised, and connectivity across/along river channels is significantly enhanced.

Additionally, dark eolian dust zones pose a substantial challenge for supraglacial river detection. In our test sites, these dark zones expand greatly in the July 31 images (see Fig. 6). Dark dusts have very similar spectral characteristics to rivers and thus hinder effective river delineation (see Fig. 6(f) and (h)). Supraglacial rivers cannot be confidently delineated in such zones. A zoom-in view of Site 4 further illustrates this point (see Fig. 7). A dark eolian dust zone expands significantly at the bottom of the July 31 image, and rivers located in this zone are not delineated. At the top of the July 31 images, rivers are dry and show very low contrast with the ice surface background, resulting in poor delineation.

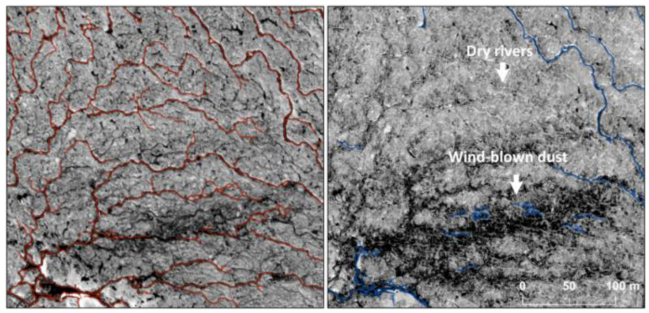

Fig. 7. Rapid changes in GrIS surface (left: July 18 image, and right: July 31 image), caused by concentration of eolian (wind-blown) dust from GrIS ablation and surface runoff processes. Supraglacial river networks also declined over this period leading to dry channels.

E. Supraglacial River Registration Results

The proposed method demonstrates robust registration performance in all of the four test sites. Fig. 8 shows that spatial offsets among TPs in the master and slave images are significantly eliminated. The majority of river points in the slave images are successfully matched to the corresponding locations in the master images, with the resultant RMSE below 3.0 m (see Table I). Some example zoomed-in views are presented in Fig. 9, which indicates that the registered slave images match very well with the master images. This suggests that the registered images are useful for investigating ice surface dynamics due to their good spatial accuracy.

The proposed method performs the best when no significant changes occur on the ice surface. For example, the July 24 river networks for Site 1 are very similar to the corresponding July 18 river networks (see Fig. 6(a) and (b)), thus yielding a small RMSE = 1.18 m. The accuracy of the proposed method

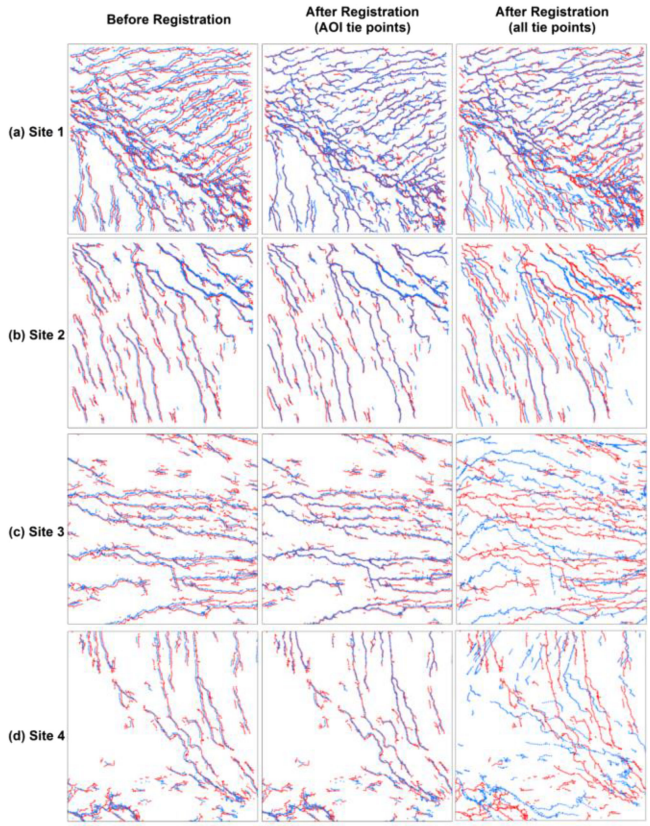

Fig. 8. Registration of supraglacial rivers for Sites 1–4. Column 1 shows spatial offsets between July 18 river TPs (red) and July 24 or 31 river TPs (blue). If only the TPs located in AOI are used, these spatial offsets are successfully eliminated after registration (column 2). However, if all the TPs obtained from Fig. 7 are used, registration fails and larger spatial offsets are generated (column 3).

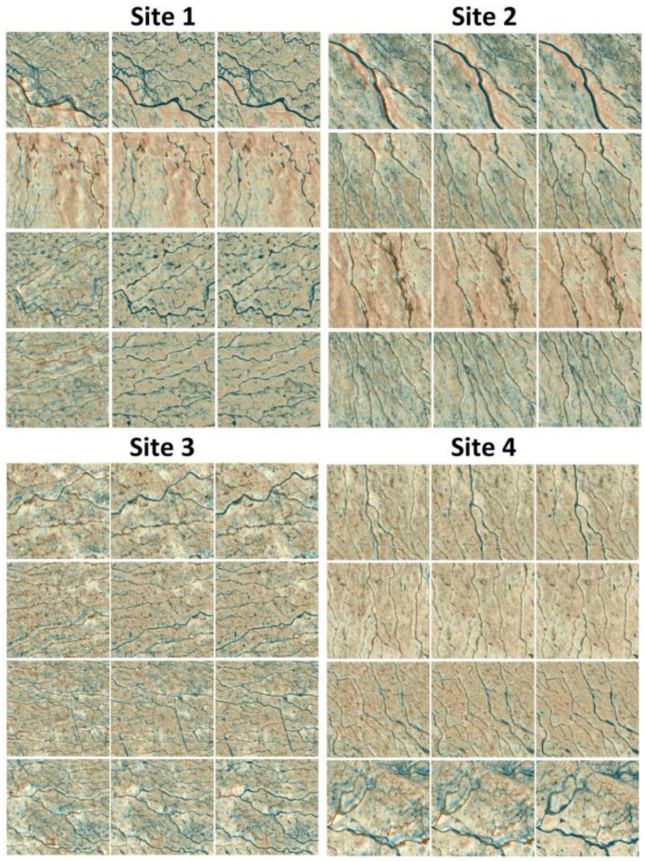

Fig. 9. Example zoomed images showing the registration results for Sites 1–4. For each test site, the first column shows the overlaid master and slave images prior to registration, the second column shows the result after registration using the described method, and the third column shows the result after manual registration.

decreases when considerable changes occur on the ice surface. For Site 2, numerous rivers dry up after July 18 and are therefore not delineated in the July 31 image (see Fig. 6(c) and (d)); however, it is still possible to determine the overall river pattern and temporal changes are moderate. As such, the resultant RMSE of 1.69 m is relatively small. In contrast, both the ice surface and associated river networks change substantially at Sites 3 and 4 (see Fig. 6(e)–(h)), and the resultant RMSE increases to 2.42 and 2.80 m, respectively. One reason is that rivers are completely or almost drained in some areas of Sites 3 and 4 (e.g., top part of Site 3 and left part of Site 4) and consequently are not delineated in the July 31 image (see Figs. 6 and 8). Manual validation points located in these places contribute to large RMSE (4.21 m for Site 3 and 4.94 m for Site 4). If these points are eliminated from the validation group, the RMSEs for Sites 3 and 4 decrease to 1.77 and 2.08 m, respectively.

In general, the proposed method presents good registration accuracy, comparable with the manual method (see Table I). At Site 1, supraglacial river networks are stable and thus numerous correct TPs are created, yielding a better registration result (RMSE $=$ 1.18 m) than the manual method (RMSE $=$ 1.32 m). At Site 2, the ice surface changes moderately, while the overall pattern of the river networks is relatively stable. The resultant RMSE (1.69 m) is slightly larger than the corresponding RMSE (1.32 m) obtained from the manual method. At Sites 3 and 4, the ice surface changes dramatically but the proposed method performs satisfactorily, yielding comparable RMSE (2.42 and 2.80 m) with the manual method (1.86 and 2.03 m). Considering that manually delineating TPs from the ice surface is time consuming and subject to errors, particularly for areas where significant surface changes occur (e.g., Sites 3 and 4), the proposed method is an accurate and more practical approach for the automated registration of high-resolution ice surface images.

The four comparison image registration methods cannot be applied to ice surface when significant temporal changes occur (see Fig. 10). At Site 1, the SURF method successfully detects 90 matching point pairs; the other three methods detect $\sim$10 matching point pairs (see Table II). However, all the matching pairs are located in the upper right part of the two images where ice surface is very similar during July 18–24. The bottom left parts of the two images represent considerable changes (see Figs. 6 and 8) and all the four registration methods fail to identify matching pairs there. At Site 2, ice surface change is moderate and the SURF method detects 7 matching pairs, all of which are located in the upper right parts of the two images; the other three methods fail to detect correct matching pairs. At Sites 3 and 4, ice surface changes substantially and all the

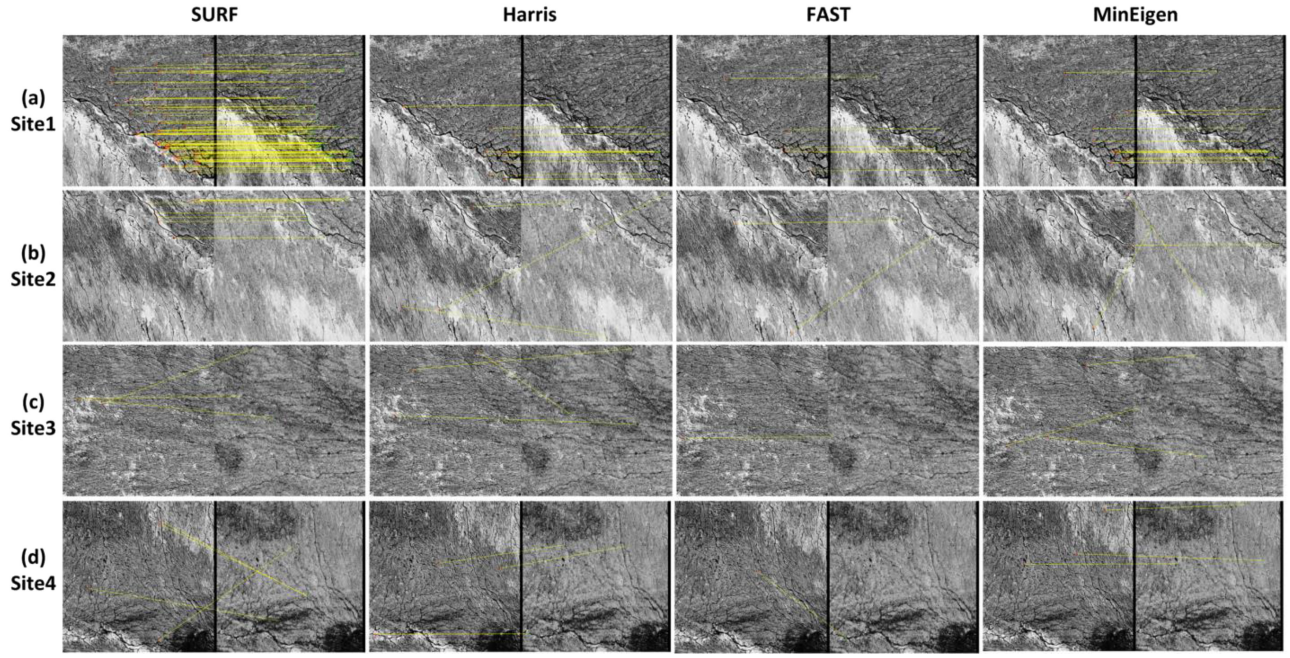

Fig. 10. Matching results for Sites 1–4 using four comparison image registration methods. The numbers of correct matching point pairs are shown in Table II.

TABLE II
NUMBER OF CORRECT MATCHING POINT PAIRS FOR SITES 1–4 USING FOUR COMPARISON IMAGE REGISTRATION METHODS

	SURF	Harris	FAST	MinEigen
Site 1	90	12	6	13
Site 2	7	0	0	1
Site 3	1	0	1	0
Site 4	0	2	0	1

four comparison registration methods fail to match the two image pairs [see Fig. 10(c) and (d) and Table II]. For all the four test sites, most of the correct matching pairs, notably, are located at edges of supraglacial river channels or small meltwater ponds. This further confirms the conclusion that supraglacial rivers are pervasive features in the GrIS high-resolution images during melt seasons [23]. In sum, the highly dynamic pattern of those meltwater rivers and the ice surface background leads to poor performances of those four comparison image registration methods.

F. Controlling Factors for Image Registration Accuracy

Creating an AOI by buffer and overlay operations is found to be a crucial process in conducting successful registration of the dynamic ice surface images. Fig. 8 shows the registration results using the TPs located in the AOI and using all TPs created from rivers. The results show that performance is enhanced when the AOI pie points are used, as opposed to all of the TPs. The input master and slave river networks at Site 1 are similar to each other so using all the TPs yields an acceptable registration for most parts of the image; however, considerable offsets are observed in the bottom left of the image where the input river networks are different. For Sites 2–4, river networks are erroneously registered, yielding larger spatial offsets than the ones among input river networks. This is mainly because supraglacial river networks change greatly from July 18 to 31 at Sites 2–4 and numerous erroneous TPs are included in the registration if an AOI is not applied. Therefore, in this study, the AOI is crucial to conduct successful registration, which implies that the spatial distribution of supraglacial river networks and their temporal variations have important impacts on the accuracy of image registration.

To further illustrate this impact, the TP ratio R_{tp} is used here as a quantitative metric (see Fig. 11). Supraglacial rivers delineated from the July 18 images (the master images) are better developed than those rivers from the July 24 and the July 31 images (the slave images) (see Fig. 6 and Table I). Therefore, R_{tp} values obtained in this study are all smaller than 1.0 (see Table I). A larger R_{tp} indicates that the two TP sets used to conduct CPD registration are more alike. It also means that fewer changes occur on the ice surface and fewer outliers are included in the CPD registration (see Fig. 8). As such, the proposed method is expected to perform better when R_{tp} is larger. A strong negative linear relationship ($R^2 = 0.98$) between R_{tp} and RMSE is found and consequently supports this assumption (see Fig. 11(a)). More specifically, R_{tp} values for Sites 1 and 2 are large ($>$0.90), indicating that rivers delineated from the master and slave images are similar; therefore, the majority of TPs included in the registration are true positives and advocate the good performance of the CPD registration [35]. However, R_{tp} values for Sites 3 and 4 are smaller ($<$0.80), indicating that a considerable number of TPs included in the registration are outliers. These outliers reduce the accuracy of registration and contribute to larger RMSE values. For example, at Site 3, supraglacial rivers are very well defined in the July 18

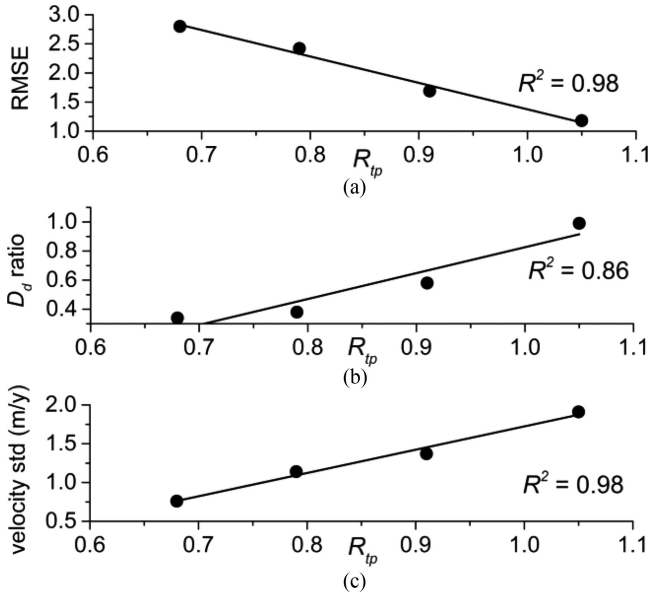

Fig. 11. TP ratio ($R_{\rm tp}$) versus (a) RMSE of registration and (b) drainage density (D_d) ratio, and (c) standard deviation (Std) of ice flow velocity.

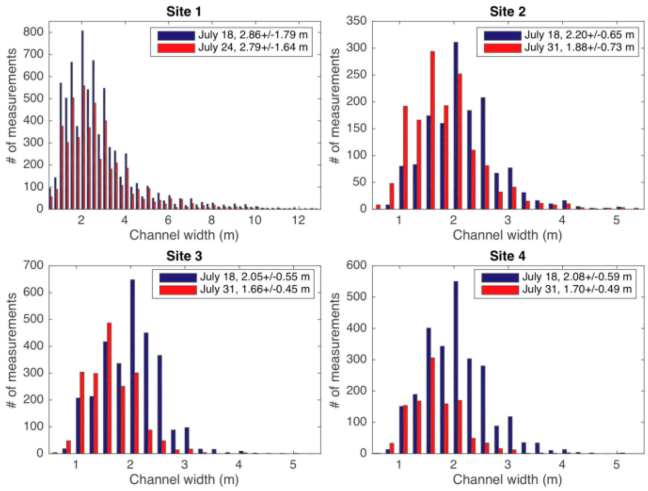

Fig. 12. Histograms of remotely sensed supraglacial channel width for Sites 1–4. Peak channel widths are stable over the period July 18–24 (Site 1). Between July 24 and 31, channel widths narrow in response to declining meltwater production on the GrIS surface (Sites 2–4).

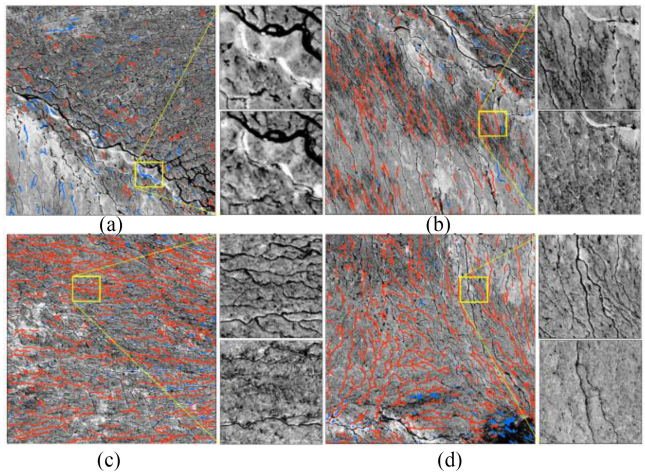

Fig. 13. Histograms of remotely sensed supraglacial channel width for Sites 1–4. Peak channel widths are stable over the period July 18–24 (Site 1). Between July 24 and 31, channel widths narrow in response to declining meltwater production on the GrIS surface (Sites 2–4).

image ($D_d = 58.1$ km/km^2) and the spaces among channels are small, while over 60% of the rivers disappear in the July 31 image ($D_d = 21.8$ km/km^2). However, numerous July 18 river points are still included in the AOI even though these points have no associated July 31 river points, consequently performing as outliers in the registration. Finally, $R_{\rm tp}$ is found to positively correlate with the drainage density ratio ($R^2 = 0.86$, Fig. 11(b)). This is predictable because the TPs included in the AOI for the master and slave images are more similar when the drainage densities of these two images are also more alike (see Table I). Notably, $R_{\rm tp}$ equals the D_d ratio if the buffer and overlay operations are not conducted.

G. Implications for Supraglacial Hydrology

Well-registered ice surface images can be used to study the evolution of supraglacial hydrology [9]. Results show that supraglacial river networks are well developed on 18 July 2015, with the resultant drainage density ranging from 47.0 to 52.1 km/km^2. In contrast, the drainage density on July 31 decreases greatly, ranging from 15.8 to 22.2 km/km^2 (see Table I), showing an average decrease of 59.3% and thus indicating substantial ice surface changes. These changes are mainly because surface runoff reduces from 2.7 cm on July 18 to 1.6 cm on July 31 (runoff is calculated from the MAR), an overall decrease of 40.7%. Numerous supraglacial channels dry up due to insufficient meltwater supply (see Fig. 6). Meanwhile, supraglacial rivers become narrower, their width decreasing from 2.1–2.8 m on July 18 to 1.7–1.9 m on July 31 (see Table I). The histograms of river width at four sites show this narrowing process clearly (see Fig. 12). Peak width stays the same from July 18 to 24 (Site 1), whereas it decreases on July 31 (Sites 2–4).

The overall pattern of supraglacial river networks is stable from July 18 to 24 (see Fig. 6(a) and (b), and Fig. 8(a)), mainly due to efficient meltwater supply (surface runoff is 2.6 cm on July 24). This conclusion is also supported by stable drainage density and river width during this period (see Fig. 12 and Table I). However, considerable detail changes can be observed. At the bottom-left part of Site 1, some new meltwater channels form in bright snow patches (see Fig. 13(a)). This reveals that meltwater rivers are better channelized as surface melt increases, which has been reported in [5]. In addition, reuse of abandoned channels (see the zoom-in view of Fig. 13(a)) and melting of ice bridges also contribute to new channel formation. In contrast, at the upper-right part of Site 1, some headwater channels disappear. This implies that those small channels are very sensitive to meltwater supply decreasing (~ 0.1 cm/day). Notably, those small headwater channels may not dry up completely; instead, they may only become too narrow (e.g., $\sim$0.1 m or less) to be

detected in 0.5 m WV panchromatic imagery [29]. Sites 2–4 show significant changes of supraglacial river networks from July 18 to 31 (see Fig. 13(b)–(d)). Most of meltwater tributaries dry up, whereas trunk meltwater channels are relatively stable. This is predictable because those trunk channels have large contributing drainage areas [23] and are thus more likely to remain active.

This temporal evolution reveals a strong relationship between the surface melt intensity and the supraglacial river drainage network of the GrIS. As a melt season proceeds and surface melt decreases, small headwater channels dry up (or become much narrower) and meltwater tributaries start to shrink. Meltwater trunk channels may remain active (but generally become narrower) until late summer due to their larger contributing areas [23], which is also supported by the observation in [24].

H. Implications for Ice Flow

Although there are clear signs of stream advection by ice flow [9], no significant relationship between ice flow and supraglacial river changes is found over the short timescales considered in this study. Table I shows the mean ice flow velocities and their standard deviations at four test sites. If ice flow velocity and its spatial variations have considerable impacts on the pattern changes in supraglacial river networks, larger and more variable spatial offsets among river networks will be obtained, manifested by a negative relationship between velocity and R_{tp}. However, this relationship is not identified (see Table I). In contrast, we find a positive correlation between R_{tp} and the standard deviation of ice flow velocity ($R^2 = 0.77$, Fig. 11(c)). This suggests that more variable ice flow velocities do not necessarily induce larger changes in supraglacial river network patterns. One possible explanation is that ice-flow-induced supraglacial river changes are too weak to distinguish with the raw spatial offsets during a short study period (e.g., $\sim$10 days in this study, which translates to $\sim$2 m advection of passive tracers using mean local ice velocities from Table I), or that more features are necessary to constrain the surface ice velocity vector field.

IV. Conclusion

The proposed method has two areas for improvement. First, the performance of the proposed method declines when supraglacial river networks delineated from two separate dates differ substantially because some outliers are included in registration even after AOI processing. Therefore, further refinement is required to select more robust TPs for registration. Second, the proposed method relies on the similarity of supraglacial rivers over short-term periods, and thus the registered images can only be used to illustrate short-term dynamics on the ice surface. However, it is also important to analyze long-term (e.g., multiple melt seasons) ice surface dynamics. The proposed method will fail to register ice surface images if the associated river networks are extremely different. We do not attempt to derive a reliable metric for requisite image similarity here. It will depend on a combination of the local ice velocity, position in any larger scale supraglacial drainage basin (including the stability of drainage divides), and melt rate. Of course, ice flow plays a key role in long-term (seasonal or annual) river evolution that is expressed through ice surface images and the time evolving melt supply. Regional ice velocity models may therefore be constrained if the influence of ice flow on stream dynamics is better understood. Extending these methods to time periods over which ice advection is significant is left to future work.

High-resolution satellite imagery has been widely used in GrIS studies. However, it is challenging to register these ice surface images because surface features are difficult to delineate and significant changes occur on the ice surface. This study proposes a new automated method to register high-resolution ice surface images using supraglacial rivers. The main contribution of this method is, first, that it constitutes an effective approach for delineating supraglacial rivers from variable ice surface backgrounds. Variable ice surface backgrounds are successfully eliminated by spectral analysis and nonlocal means denoising. Small supraglacial rivers are effectively enhanced by Gabor filtering and continuous supraglacial river networks are obtained by path opening. Second, a combination of two GIS tools, i.e., buffer and overlay, constrains the delineated rivers and yields useful TPs for registration. Experimental results show that the proposed method yields comparable performances to manual registration. Given the difficulties with identifying stable features on the ice surface, the proposed method can be an effective way of processing high-resolution satellite images of the ice surface. The well-registered images can then be applied to study the hydrological/glaciological processes on the ice surface.

Acknowledgment

The authors would like to thank the Polar Geospatial Center, University of Minnesota, for providing WorldView imagery, M. Tedesco for providing Modèle Atmosphérique Régional climate model v3.6, and T. Nagler for providing Sentinel-1 ice flow velocity dataset. They also thank the detailed and constructive comments on this manuscript from both reviewers and editor.

References

[1] E. Hanna *et al.*, "Ice-sheet mass balance and climate change," *Nature*, vol. 498, no. 7452, pp. 51–59, 2013.

[2] M. Van den Broeke *et al.*, "Partitioning recent Greenland mass loss," *Science*, vol. 326, no. 5955, pp. 984–986, 2009.

[3] V. W. Chu, "Greenland ice sheet hydrology: A review," *Prog. Phys. Geography*, vol. 38, no. 1, pp. 19–54, 2014.

[4] A. K. Rennermalm *et al.*, "Understanding Greenland ice sheet hydrology using an integrated multi-scale approach," *Environ. Res. Lett.*, vol. 8, no. 1, 2013, Art. no. 015017.

[5] K. Yang and M. Li, "Greenland ice sheet surface melt: A review," *Sci. Cold Arid Reg.*, vol. 6, no. 2, pp. 99–106, 2014.

[6] K. Yang and L. C. Smith, "Supraglacial streams on the Greenland ice sheet delineated from combined spectral-shape information in high-resolution satellite imagery," *IEEE Geosci. Remote Sens. Lett.*, vol. 10, no. 4, pp. 801–805, Jul. 2013.

[7] L. Karlstrom, A. Zok, and M. Manga, "Near-surface permeability in a supraglacial drainage basin on the Llewellyn Glacier, Juneau Icefield, British Columbia," *Cryosphere*, vol. 8, no. 2, pp. 537–546, 2014.

[8] N. Selmes, T. Murray, and T. D. James, "Fast draining lakes on the Greenland ice sheet," *Geophys. Res. Lett.*, vol. 38, no. 15, 2011, Art. no. L15501.

[9] L. Karlstrom and K. Yang, "Fluvial supraglacial landscape evolution on the Greenland ice sheet," *Geophys. Res. Lett.*, vol. 43, no. 6, pp. 2683–2692, 2016.

[10] L. C. Smith *et al.*, "Efficient meltwater drainage through supraglacial streams and rivers on the southwest Greenland ice sheet," *Proc. Nat. Acad. Sci. USA*, vol. 112, no. 4, pp. 1001–1006, 2015.
[11] I. G. M. Wientjes and J. Oerlemans, "An explanation for the dark region in the western melt zone of the Greenland ice sheet," *Cryosphere*, vol. 4, no. 3, pp. 261–268, 2010.
[12] J. Ettema *et al.*, "Higher surface mass balance of the Greenland ice sheet revealed by high-resolution climate modeling," *Geophys. Res. Lett.*, vol. 36, no. 12, 2009, Art. no. L12501.
[13] I. Joughin, B. E. Smith, I. M. Howat, T. Scambos, and T. Moon, "Greenland flow variability from ice-sheet-wide velocity mapping," *J. Glaciol.*, vol. 56, no. 197, pp. 415–430, 2010.
[14] B. Zitova and J. Flusser, "Image registration methods: A survey," *Image Vis. Comput.*, vol. 21, no. 11, pp. 977–1000, 2003.
[15] Y. Sheng, C. A. Shah, and L. C. Smith, "Automated image registration for hydrologic change detection in the lake-rich Arctic," *IEEE Geosci. Remote Sens. Lett.*, vol. 5, no. 3, pp. 414–418, Jul. 2008.
[16] Q. Li, G. Wang, J. Liu, and S. Chen, "Robust scale-invariant feature matching for remote sensing image registration," *IEEE Geosci. Remote Sens. Lett.*, vol. 6, no. 2, pp. 287–291, Apr. 2009.
[17] D. Bhattacharya and S. Sinha, "Invariance of stereo images via the theory of complex moments," *Pattern Recognit.*, vol. 30, no. 9, pp. 1373–1386, 1997.
[18] G. Stockman, S. Kopstein, and S. Benett, "Matching images to models for registration and object detection via clustering," *IEEE Trans. Pattern Anal. Mach. Intell.*, vol. PAMI-4, no. 3, pp. 229–241, May 1982.
[19] H. Sui, C. Xu, J. Liu, and F. Hua, "Automatic optical-to-SAR Image registration by iterative line extraction and Voronoi integrated spectral point matching," *IEEE Trans. Geosci. Remote Sens.*, vol. 53, no. 11, pp. 6058–6072, Nov. 2015.
[20] F. Dellinger, J. Delon, Y. Gousseau, J. Michel, and F. Tupin, "SAR-SIFT: A SIFT-like algorithm for applications on SAR images," in *Proc. 2012 IEEE Int. Geosci. Remote Sens. Symp.*, 2012, pp. 3478–3481.
[21] X. Dai and S. Khorram, "A feature-based image registration algorithm using improved chain-code representation combined with invariant moments," *IEEE Trans. Geosci. Remote Sens.*, vol. 37, no. 5, pp. 2351–2362, Sep. 1999.
[22] A. Marsetic, K. Ostir, and M. K. Fras, "Automatic orthorectification of high-resolution optical satellite images using vector roads," *IEEE Trans. Geosci. Remote Sens.*, vol. 53, no. 11, pp. 6035–6047, Nov. 2015.
[23] K. Yang *et al.*, "Fluvial morphometry of supraglacial river networks on the southwest Greenland ice sheet," *GIsci. Remote Sens.*, vol. 53, no. 4, pp. 459–482, 2016.
[24] D. J. Lampkin and J. VanderBerg, "Supraglacial melt channel networks in the Jakobshavn Isbræ region during the 2007 melt season," *Hydrol. Processes*, vol. 28, no. 25, pp. 6038–6053, 2014.
[25] T. Phillips *et al.*, "Modeling moulin distribution on Sermeq Avannarleq glacier using ASTER and WorldView imagery and fuzzy set theory," *Remote Sens. Environ.*, vol. 115, no. 9, pp. 2292–2301, 2011.
[26] R. Walker and J. Jackson, "Offset and evolution of the Gowk fault, S.E. Iran: A major intra-continental strike-slip system," *J. Struct. Geol.*, vol. 24, no. 11, pp. 1677–1698, 2002.
[27] S. Jeong and I. M. Howat, "Performance of Landsat 8 operational land imager for mapping ice sheet velocity," *Remote Sens. Environ.*, vol. 170, pp. 90–101, 2015.
[28] D. M. Rippin, A. Pomfret, and N. King, "High resolution mapping of supra-glacial drainage pathways reveals link between micro-channel drainage density, surface roughness and surface reflectance," *Earth Surf. Process. Landforms*, vol. 40, no. 10, pp. 1279–1290, 2015.
[29] L. Karlstrom, P. Gajjar, and M. Manga, "Meander formation in supraglacial streams," *J. Geophys. Res. Earth Surf.*, vol. 118, no. 3, pp. 1897–1907, 2013.
[30] J. T. Perron, J. W. Kirchner, and W. E. Dietrich, "Spectral signatures of characteristic spatial scales and nonfractal structure in landscapes," *J. Geophys. Res. Earth Surf.*, vol. 113, no. F4003, 2008.
[31] P. Coupe, P. Hellier, C. Kervrann, and C. Barillot, "Nonlocal means-based speckle filtering for ultrasound images," *IEEE Trans. Image Process.*, vol. 18, no. 10, pp. 2221–2229, Oct. 2009.
[32] L. N. Darlow, S. S. Akhoury, and J. Connan, "A review of state-of-the-art speckle reduction techniques for optical coherence tomography fingertip scans," in *Proc. 7th Int. Conf. Mach. Vis.*, Milan, Italy, vol. 9445, no. 944523, 2015.
[33] K. Yang, M. Li, Y. Liu, L. Cheng, Q. Huang, and Y. Chen, "River detection in remotely sensed imagery using Gabor filtering and path opening," *Remote Sens.*, vol. 7, no. 7, pp. 8779–8802, 2015.
[34] K. Yang, L. C. Smith, V. W. Chu, C. J. Gleason, and M. Li, "A caution on the use of the digital elevation models to simulate supraglacial hydrology of the Greenland ice sheet," *IEEE J. Sel. Topics Appl. Earth Observ. Remote Sens.*, vol. 8, no. 11, pp. 5212–5224, Nov. 2015.
[35] A. Myronenko and X. B. Song, "Point set registration: Coherent point drift," *IEEE Trans. Pattern Anal. Mach. Intell.*, vol. 32, no. 12, pp. 2262–2275, Dec. 2010.
[36] X. Fettweis *et al.*, "Estimating the Greenland ice sheet surface mass balance contribution to future sea level rise using the regional atmospheric climate model MAR," *Cryosphere*, vol. 7, no. 2, pp. 469–489, 2013.
[37] C. L. Vernon *et al.*, "Surface mass balance model intercomparison for the Greenland ice sheet," *Cryosphere*, vol. 7, no. 2, pp. 599–614, 2013.
[38] T. Nagler, H. Rott, M. Hetzenecker, J. Wuite, and P. Potin, "The sentinel-1 mission: New opportunities for ice sheet observations," *Remote Sens.*, vol. 7, no. 7, pp. 9371–9389, 2015.
[39] F. Isikdogan, A. Bovik, and P. Passalacqua, "Automatic channel network extraction from remotely sensed images by singularity analysis," *IEEE Geosci. Remote Sens. Lett.*, vol. 12, no. 11, pp. 2218–2221, Nov. 2015.
[40] A. F. Frangi, W. J. Niessen, K. L. Vincken, and M. A. Viergever, "Multiscale vessel enhancement filtering," in *Proc. 1st Int. Conf. Med. Image Comput. Comput.-Assisted Intervention*, Cambridge, MA, USA, 1998, pp. 130–137.
[41] S. Chaudhuri, S. Chatterjee, N. Katz, M. Nelson, and M. Goldbaum, "Detection of blood vessels in retinal images using two-dimensional matched filters," *IEEE Trans. Med. Imag.*, vol. 8, no. 3, pp. 263–269, Sep. 1989.
[42] K. Yang, M. Li, Y. Liu, Y. Duan, and M. Zhou, "River delineation from remotely sensed imagery using a multi-scale classification approach," *IEEE J. Sel. Topics Appl. Earth Observ. Remote Sens.*, vol. 7, no. 12, pp. 4726–4737, Dec. 2014.
[43] H. Bay, A. Ess, T. Tuytelaars, and L. Van Goola, "Speeded-up robust features (SURF)," *Comput. Vis. Image Understanding*, vol. 110, no. 3, pp. 346–359, Jun. 2008.
[44] C. Harris and M. Stephens, "A combined corner and edge detector," in *Proc. 4th Alvey Vis. Conf.*, 1988, pp. 147–151.
[45] E. Rosten and T. Drummond, "Fusing points and lines for high performance tracking," in *Proc. 10th IEEE Int. Conf. Comput. Vis.*, 2005, pp. 1508–1515.
[46] J. Shi and C. Tomasi, "Good features to track," in *Proc. IEEE Conf. Comput. Vis. Pattern Recognit.*, 1994, pp. 593–600.

Kang Yang received the Ph.D. degree in Geography from Nanjing University, Nanjing, China, in 2014.

He is currently a Postdoctoral Scholar in the Department of Geography, University of California, Los Angeles, Los Angeles, CA, USA. His research interests include Greenland ice sheet hydrology and river remote sensing.

Leif Karlstrom received the Ph.D. degree in Earth and Planetary Sciences from the University of California, Berkeley, Berkeley, CA, USA, in 2011.

He is currently an Assistant Professor in the Department of Earth Sciences, University of Oregon, Eugene, OR, USA. His research interests include volcanology, glaciology, and landscape evolution.

Laurence C. Smith received the Ph.D. degree in Earth and Atmospheric Sciences from Cornell University, Ithaca, NY, USA, in 1996.

He is currently a Professor and Chair of Geography and a Professor of Earth, Planetary, and Space Sciences at the University of California, Los Angeles, Los Angeles, CA, USA. His research interests include the Arctic, hydrology, satellite remote sensing technologies, and climate change.

Dr. Smith was named a Guggenheim Fellow by John S. Guggenheim Foundation in 2006 and 2007. In 2015, he was elected Fellow of the American Geophysical Union.

Manchun Li received the Ph.D. degree in Cartography from Nanjing University, Nanjing, China, in 1992.

He is currently a Professor in the Department of Geographic Information Science, Nanjing University. His research interests include geographic information system and remote sensing applications.